8

e^+e^- physics and the standard model

The recent story of narrow resonance discoveries (see Chapter 11) has shown how the properties of systems with quantum numbers of the photon (1^{--}) can best be studied with e^+e^- colliders. In this chapter we review some of the information that has come from e^+e^- machines. In particular, we shall see what support they provide for the SM. We also discuss the perspective for future e^+e^- colliders.

8.1 Electron–positron storage rings

The ideal tools for studying the spectroscopy of the new vector meson particles have undoubtedly been the various e^+e^- colliding beam machines: SPEAR at SLAC, DORIS at DESY (Deutsches Elektronen Synchrotron), PETRA at DESY and, more recently, SLC at Stanford and LEP 1 at CERN though the actual discovery (Aubert *et al.*, 1974; Herb *et al.*, 1977; UA1, 1983; UA2, 1983) of some of these particles occurred on the proton machines (Brookhaven, Fermilab and CERN).

The reason for the latter lies in the narrowness of these particles; one can simply miss them as one varies the energy. On the other hand, once discovered, the fact that $J/\Psi(3097)$, $\Upsilon(9.46)$ and the Z are vector particles 1^{--}, and thus couple naturally to a virtual photon, makes an e^+e^- machine particularly efficacious since the main channel of e^+e^- annihilation is into a virtual photon.

Thus, it is rather difficult in an e^+e^- machine to sit right on top of one of these very narrow resonances whose width may be much smaller than the energy resolution of the machine itself. On the other hand, once the mass of a narrow resonance is known, an e^+e^- machine can be tuned to the right energy to obtain an extremely large number of events.

In a hadronic machine, the reaction not only does not proceed uniquely through the 1^{--} channel, but the 1^{--} states are produced together with a

lot of other particles. Thus, once a particular decay channel (like e^+e^- or $\mu^+\mu^-$) is selected, and the centre-of-mass energy is above the production threshold, the resonance is produced over all the available phase space and a narrow peak gets smeared out into a broader bump.

The rôle of e^+e^- machines has been so important in the development of the new narrow resonance spectroscopy as to merit a short digression on their origin, their kinematics, some of their properties and some of their achievements.

Colliding-beam e^+e^- machines were first advocated by B. Touschek in the late fifties, but not even the greatest optimist could have foreseen the development that took place after the early days of the single ring device ADA (Anello Di Accumulazione) whose operation began in 1960.

In an e^+e^- machine there is no distinction between 'beam' and 'target' particles, and each beam has about the same density of particles (typically, 10^8-10^{12} particles per beam depending on the kind of particle). In a fixed-target machine, the density of particles in the target is of course much higher. Thus, to have a comparable rate of events, in an e^+e^- machine particles must be accumulated for hours (which corresponds to billions of revolutions) and this is the reason for the 'storage ring' approach.

One of the greatest advantages of colliding-beam devices as compared with conventional fixed-target accelerators is, of course, the enormous gain in energy that one obtains. A further advantage of e^+e^- machines, in particular, is that for hadronic production at least at the leptonic vertex, the reaction is supposed to be understood since at lower energies one virtual photon exchange, and at higher energies, photon and Z^0 exchanges dominate so that a reaction proceeds essentially as shown:

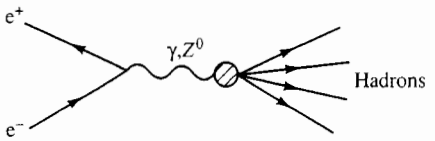

Furthermore, at low energies the quantum numbers J^{PC} of the final state are well defined being those of the photon 1^{--}. In this case, the analysis of the final state is not obscured by the need to separate the various contributions that would be present in channels involving hadrons (as, for instance, in pp or $p\bar{p}$ colliders). At higher energies the final state still has $J = 1$ but its parity is not determined on account of Z^0 exchange.

When the final state is simply a hadron–antihadron pair, $h\bar{h}$, one has a direct measurement of the hadron's electromagnetic form factor in the time-like region.

Let m_i, $\boldsymbol{p}_i$ and E_i $(i = 1, 2)$ be the masses, momenta and energies of the initial particles in the LAB. Since the LAB and CM essentially coincide,

the total CM energy is given by

$$E_{CM}^2 = (E_1 + E_2)^2 - (\boldsymbol{p}_1 + \boldsymbol{p}_2)^2 = m_1^2 + m_2^2 + 2(E_1E_2 - \boldsymbol{p}_1 \cdot \boldsymbol{p}_2). \quad (8.1.1)$$

For head-on collisions ($\boldsymbol{p}_1 = -\boldsymbol{p}_2, E_1 = E_2 = E$) we have

$$E_{CM} = 2E. \quad (8.1.2)$$

Compare this with a fixed-target collision ($\boldsymbol{p}_2 = 0, E_2 = m_2$) where we would have, at high energy,

$$E_{CM}^2 = m_1^2 + m_2^2 + 2m_2E \simeq 2m_2E. \quad (8.1.3)$$

Thus, as an example, to attain the equivalent maximum CM energy of $\simeq 100$ GeV at which the e^+e^- machine LEP 1 operates, one would need an e^+ beam striking a stationary target at an energy of approximately 10^7 GeV!

As already mentioned, the shortcoming of a collider as compared with a fixed-target accelerator lies in the intensity, whose measure in a storage ring is given by the *luminosity*. For a given reaction, this is defined as the rate of interactions per unit cross-section

$$\text{Rate} = L\sigma \equiv N. \quad (8.1.4)$$

If n_i $(i = 1, 2)$ are the number of particles per bunch, f is the frequency of revolution, b the number of bunches per beam and A the transverse area of the beam, the event rate is given by

$$N = \frac{n_1 n_2}{A} b\sigma f = L\sigma. \quad (8.1.5)$$

For a Gaussian density distribution with transverse r.m.s. radii σ_x, σ_y we have $A = 4\pi\sigma_x\sigma_y$. If we introduce the beam currents $I_i = n_i e f b$ (e being the magnitude of the electron charge) we finally have

$$L = \frac{I_1 I_2}{e^2 b f A}. \quad (8.1.6)$$

Typical parameters for an electron–positron storage ring are $f \simeq 10^6\,\text{s}^{-1}$, $I_i \simeq 50$ mA $\simeq 3 \times 10^{17}\,e/\text{s}$, $b = 1$, $\sigma_x \simeq \sigma_y \simeq 0.03$ cm, yielding a luminosity of about $L \simeq \frac{1}{4} \times 10^{32}\,\text{cm}^{-2}\text{s}^{-1}$. With a cross-section $\sigma \simeq 1\mu b = 10^{-30}\,\text{cm}^2$, (8.1.5) leads to a (somewhat optimistic) counting rate of about $N = 25$ collisions per second.

In practice e^+e^- machines operate at luminosities between 10^{29}–10^{31} $\text{cm}^{-2}\text{s}^{-1}$ although the new generation of such devices has been planned for a maximum luminosity of 10^{32} $\text{cm}^{-2}\text{s}^{-1}$.

It is instructive to compare the previous estimate ($N \lesssim 100$ events per second for $\sigma \simeq 1\mu b$) with the corresponding rate expected for a conventional fixed-target accelerator, where

$$N = n\varrho l\sigma, \quad (8.1.7)$$

n being the number of particles per second in the beam (typically $n \simeq 10^{12}$ s^{-1}), ϱ the density of nucleons in the target and l the target length (typically $\varrho l \simeq 10^{23}$ cm^{-2}). For a cross-section $\sigma = 1\mu b$ one thus gets an estimate of $N \simeq 10^5$ events per second which would only be matched by a luminosity $L \simeq 10^{35}$ $cm^{-2}s^{-1}$! Design luminosities for the SSC (Superconducting Super Collider) in the USA and for LHC (Large Hadron Collider) at CERN are 10^{33} $cm^{-2}s^{-1}$ and $\sim 10^{34}$ $cm^{-2}s^{-1}$ respectively.

In e^+e^- colliders, the maximum luminosity is severely limited by the electromagnetic forces acting between: (i) the particles of the same beam; (ii) the particles in different beams; (iii) the particles and the ring. The luminosity varies with the beam energy E in a way which may be very different for machines of comparable energy. Typically, however, it increases with a power law between E^2 and E^4 up to a maximum energy and then decreases very steeply ($\sim E^{-10}$).

The rich physics harvest which emerged from the study of the spectroscopy of the narrow resonances owed everything to a series of gigantic detectors whose acronymic names have become part of the physics heritage (see Chapters 11 and 12).

Another important feature of e^+e^- machines is that the magnetic guide field together with the synchrotron radiation lead to transverse polarizations of the beams, with electron (positron) polarization antiparallel (parallel) to the magnetic field. The polarization arises because the synchrotron radiation induces up–down spin transitions which, for the positron, say, are larger for down→up than for up→down, where 'up' means along the guide field B.

If we start from unpolarized beams, the increase of polarization with time goes as

$$P(t) = P_0(1 - e^{-t/\tau}), \tag{8.1.8}$$

where the proportionality factor is $P_0 = 8\sqrt{3}/15 = 0.92$. The τ parameter depends on the machine parameters and on energy. The above formula is an idealization and the polarization is destroyed when the operating energy is close to so-called 'depolarizing' resonances.

8.2 The new e^+e^- colliders: TRISTAN and LEP

TRISTAN, the Japanese e^+e^- collider at KEK, has been in operation since the autumn of 1986. It began functioning with an energy of 25 GeV per beam and was upgraded reaching a CM energy $\sqrt{s} = 61.4$ GeV in the spring of 1989. There are three general purpose detectors, AMY, TOPAZ and VENUS, and one detector, SHIP, specially designed to search for highly ionizing particles. The parameters of the collider are given in Table 8.1.

	Design parameters	Achieved
Beam energy	30 GeV	30.4 GeV
Injection energy	8 GeV	8.0 GeV
Single bunch current	5 mA	4.8 mA
$2e^+ + 2e^-$ beam current	15 mA	13.6 mA
Filling time	15~20 min	20~30 min
Beam life	4~5 hr	4 hr with ~8 mA
Beam emittance	1.6×10^{-7} m rad	1.0×10^{-7} m rad
Emittance ratio, V/H	2~6%	0.5~1%
β^*_V/β^*_H	0.1 m/1.6 m	0.1 m/1.8~2 m
Peak luminosity	1.6×10^{31} cm^{-2}s^{-1}	$\sim 2\times10^{31}$ cm^{-2}s^{-1}
Integrated luminosity/day		300~ 400nb^{-1}

Table 8.1. Machine parameters for the TRISTAN e^+e^- collider.

LEP (Large Electron Positron collider) at CERN came into operation in August 1989 with a CM design energy of ~110 GeV in phase 1.

At the time of writing, LEP 1 is the great focus of excitement in the field. It was constructed to study the intermediate vector boson Z^0 which was expected to dominate e^+e^- collisions in the energy region around 90 GeV (Fig. 8.1).

A preliminary indication of this dominance is seen in the TRISTAN data on $R = \sigma(e^+e^- \to \text{hadrons})/\sigma(e^+e^- \to \mu^+\mu^-)_{QED}$ (Fig. 8.2) where $\sigma(e^+e^- \to \mu^+\mu^-)_{QED} \equiv 4\pi\alpha^2/3s$ is evaluated in (8.3.5). The final, dramatic, indication of this expectation is seen in the beautiful LEP cross-section in the Z^0 mass region in Fig. 8.2(b) (DELPHI, 1990).

The layout for LEP is shown schematically in Fig. 8.3. Note the circumference of the ring, nearly 27 km! (By comparison with the tunnel planned for SSC, however, nearly 84 km, this appears quite modest.)

LEP hosts four huge experimental detectors ALEPH, DEPHI, L3 and OPAL run by large international collaborations. (It is a sobering thought that the number of physicists, e.g. in the L3 collaboration, is 581 from 38 institutions from 13 countries at the time of writing.)

Each detector is equipped with a solenoidal magnet, central tracking chamber, electromagnetic and hadron calorimeters, muon detectors, luminosity monitor and a high degree of hermeticity. The complementary aspects of the four detectors make the whole system rather complete for a wide ranging physics programme [for a comparative analysis of the four detectors, see Thresher (1988)].

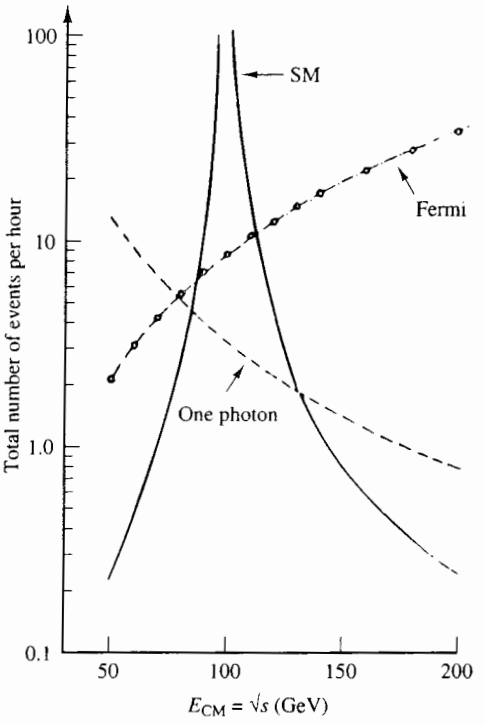

Fig. 8.1. Qualitative prediction of cross-sections for e^+e^- annihilation as a function of CM energy in the SM, the old Fermi theory and for purely electromagnetic annihilation (From Richter, 1976).

Table 8.2 gives the LEP design parameters. These correspond to between 1 and $(3\text{–}4)\times10^6$ Z^0s per year at LEP 1. In the first year of operation, 4.2×10^5 Z^0s were produced and a maximum luminosity of $6\times10^{30}\text{cm}^{-2}\text{s}^{-1}$ achieved. Increases of both energy (up to $\sqrt{s} \sim 190$ GeV) and intensity is planned in LEP 2.

Concerning polarized beams, in addition to the natural transverse polarization, spin rotation at LEP will also yield longitudinal polarization and this could prove extremely useful in allowing measurements of the weak couplings at the Z° peak with a precision otherwise unattainable. The most promising points, in this context, are the left–right asymmetry and the longitudinal polarization predictions which will be discussed in Section 8.8 and which could be the key to a substantial reduction of the experimental error on several parameters of the SM. As an example, $\sin^2\theta_W$ could be measured at LEP, without polarization, to an accuracy of 0.00033 in a 200 pb^{-1} exposure at the Z^0 peak, whereas it becomes ~ 0.00013 with 50% polarization and 30 pb^{-1}!

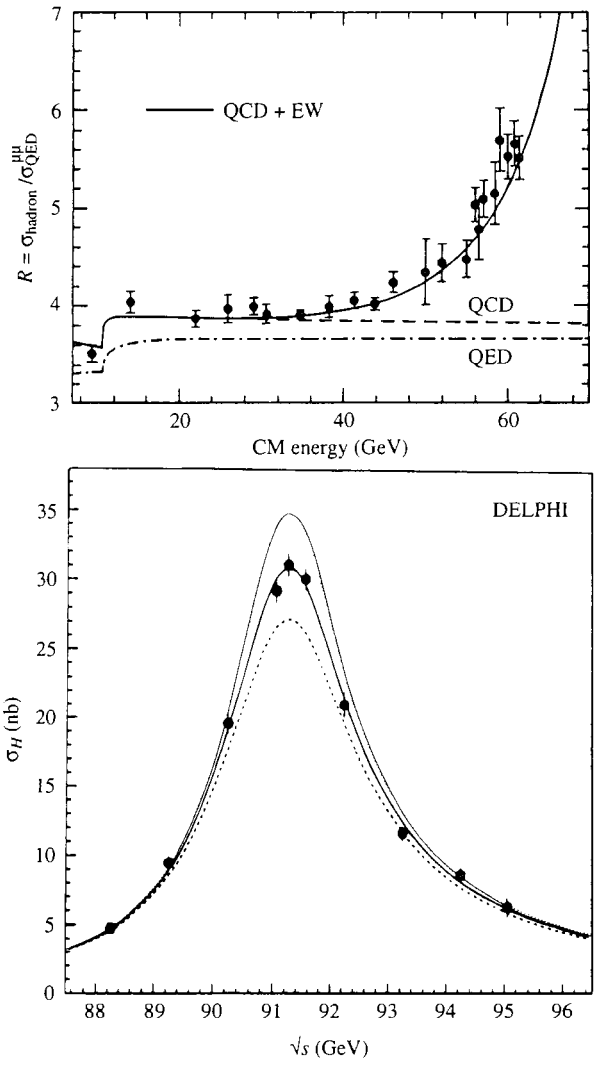

Fig. 8.2. (*a*) The prediction for the e^+e^- cross-section in the SM compared with the data from TRISTAN. The full contributions: electroweak (EW) plus QCD is shown by the continuous line. The QCD and the QED contributions are shown by dashed and dot-dashed lines respectively. (*b*) The cross-section for $e^+e^- \rightarrow$ hadrons around the Z^0 mass (DELPHI, 1990). The dotted, continuous and dashed lines are the predictions of the SM assuming two, three and four massless neutrino species respectively. (From Abe, 1991.)

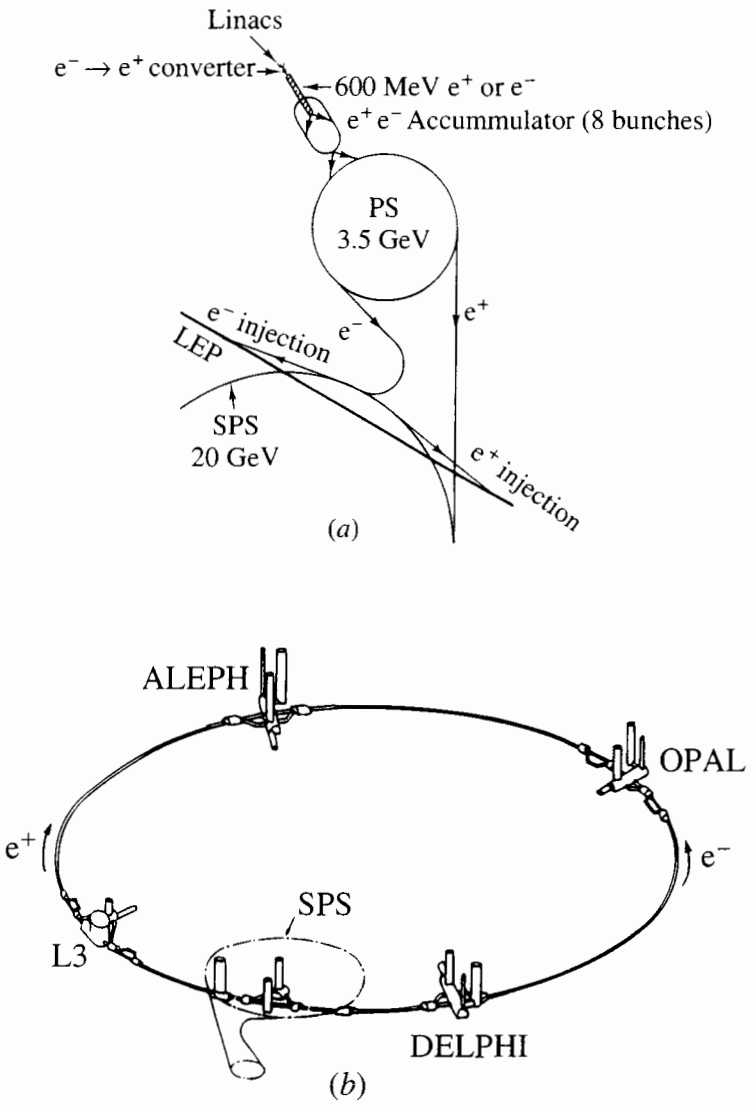

Fig. 8.3. Schematic layout of LEP (see text).

Finally, we wish to mention the Stanford Linear Collider (SLC) operating at about 100 GeV CM energy, whose first Z^0 was recorded on April 12, 1989. SLC is a single pass collider which consists of the old 3 km Stanford linac that now accelerates electrons (and positrons) to 50 GeV and two new collider arcs that bring them into head-on collision at the detector. Every other electron bunch from the injector is diverted onto a positron producing target. The low energy positron bunch is reinjected into the

	Phase 1	Phase 2
Beam energy (GeV)	55	95
Circumference (km)	26.66	26.66
Dipole field (T)	0.0645	0.1114
Injection energy (GeV)	20	20
R.F. frequency (MHz)	352	352
Dist. between supercond. quads (m)	±3.5	±3.5
r.m.s. bunch length (mm)	17.2	13.9
r.m.s. beam radii:		
σ_x (μm)	255	209
σ_y (μm)	15.3	10.8
Bunch spacing (μs)	22	22
Nom. luminosity ($cm^{-2}s^{-1}$)	1.6×10^{31}	2.7×10^{31}
Beam lifetime (h)	6	5
r.m.s. energy spread	0.92×10^{-3}	2.06×10^{-3}
Current (4 bunches) (mA)	3	3
Synchr. rad. loss per turn (GeV)	0.263	2.303

Table 8.2. LEP design parameters.

linac via a return line. Both electron and positron beams are very diffuse and are cooled radiatively in damping rings. The positron beam is then accelerated to 50 GeV by the linac and reaches the collision point just in time to collide with the next 50 GeV electron bunch. Notice that subsequent phases of the same accelerating field are used here to accelerate both e^+ and e^- bunches. The layout of SLC is shown in Fig. 8.4.

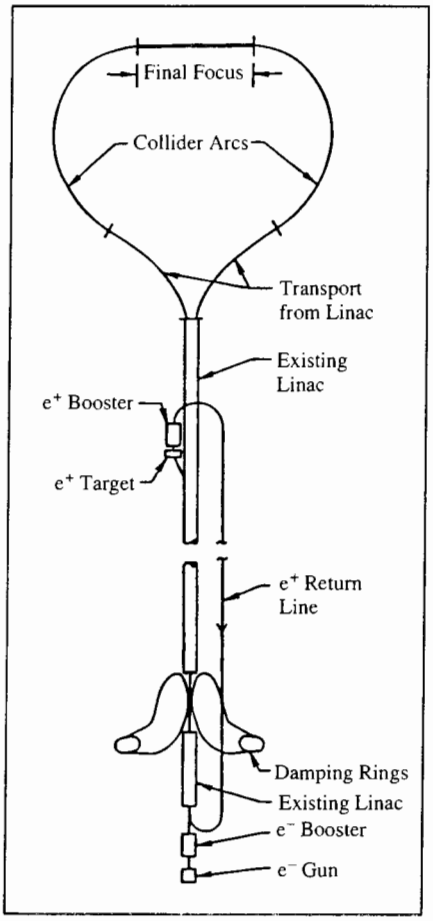

Fig. 8.4. Schematic layout of SLC (see text).

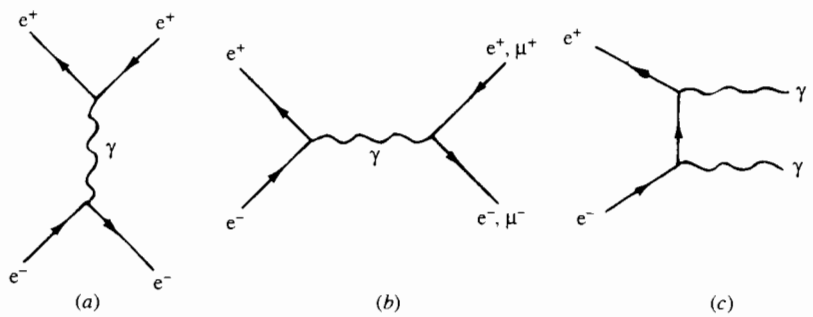

Fig. 8.5. Feynman diagrams for Bhabha scattering ($e^+e^- \to e^+e^-$), muon production ($e^+e^- \to \mu^+\mu^-$) and two-photon annihilation.